Nanoscale Res Lett (2010) 5:1228–1235
DOI 10.1007/s11671-010-9631-0

NANO IDEAS

Multiple-path Quantum Interference Effects in a Double-Aharonov-Bohm Interferometer

X. F. Yang · Y. S. Liu

Received: 10 March 2010 / Accepted: 4 May 2010 / Published online: 22 May 2010

Abstract We investigate quantum interference effects in a double-Aharonov-Bohm (AB) interferometer consisting of five quantum dots sandwiched between two metallic electrodes in the case of symmetric dot-electrode couplings by the use of the Green's function equation of motion method. The analytical expression for the linear conductance at zero temperature is derived to interpret numerical results. A three-peak structure in the linear conductance spectrum may evolve into a double-peak structure, and two Fano dips (zero conductance points) may appear in the quantum system when the energy levels of quantum dots in arms are not aligned with one another. The AB oscillation for the magnetic flux threading the double-AB interferometer is also investigated in this paper. Our results show the period of AB oscillation can be converted from 2π to π by controlling the difference of the magnetic fluxes threading the two quantum rings.

Keywords Aharonov-Bohm interferometer · Fano effects · Quantum dots · Transport properties

Thanks to rapid developments in the fabrication and self-assembly techniques, the electrical transport through nanoscale quantum systems such as a single quantum dot, multiple quantum dots, atoms or molecules coupled to metallic electrodes has been an interesting subject in recent years [1–6]. In the nanoscale quantum systems, the electrical transport is ballistic, while the phase coherence of the electrons is preserved. Especially, the quantum interference effects in an AB ring including a quantum dot have been reported [7]. The results showed that Fano effect with asymmetric parameters was a good probe to quantum interference effects in the nanoscale systems. The transport properties of a quantum ring consisting of two parallel-coupled quantum dots sandwiched between two metallic electrodes have been also studied theoretically and experimentally in the last few decades [7–22]. For example, an AB interferometer including two coupled quantum dots with each quantum dot inserted in each arm was presented, and an oscillating electric current was detected experimentally [8, 9]. Such a double-quantum-dot model consisting of the parallel-coupled double-dot system has been studied extensively in some previous theoretical works [13–18]. When the interdot coupling is considered, a bonding molecular state and an antibonding molecular state are developed. A swap effect can be found in the quantum system by tuning the magnetic flux threading the quantum ring, which may be used in the future quantum computations [15].

Recently, the transport properties of multi-parallel-coupled quantum dots have attracted considerable attention due to their potential applications and abounding physics [23–31]. Zeng et al. studied the AB effects in a quantum ring consisting of four quantum dots sandwiched between two metallic electrodes, and a Fano dip is developed when the energy levels of quantum dots in two arms are mismatched [23]. Guevara et al. offered a quantum model describing multi-parallel-coupled quantum-dot molecule, and Fano effects in the quantum system were studied in detail [24]. More recently, Li et al. studied the electrical transport through a triple-arm AB interferometer consisting of three parallel quantum dots with electron-electron interactions under an applied electric field [25].

X. F. Yang · Y. S. Liu (✉)
Jiangsu Laboratory of Advanced Functional Materials, and College of Physics and Engineering, Changshu Institute of Technology, 215500 Changshu, China
e-mail: ysliu2007@yahoo.com.cn

In this work, we study the quantum interference effects in a double-Aharonov-Bohm interferometer consisting of five quantum dots sandwiched between two metallic electrodes as shown in Fig. 1. The left quantum ring consisting of the quantum dot 1, the quantum dot 2, quantum dot 3 and the left metallic electrode encloses the magnetic flux Φ_L. The right ring consisting of the quantum dot 3, the quantum dot 4, the quantum dot 5, and the right metallic electrode encloses the magnetic flux Φ_R. Two quantum rings are connected together by the quantum dot 3. For simplicity, we consider that only one energy level exists in each quantum dot, and the energy levels of all quantum dots can be tuned by the voltages applied on the quantum dots. In this work, we studied in detail the quantum interference effects in the double-quantum-ring structure in the case of symmetric dot-electrode couplings. The results show that the linear conductance peaks at zero temperature can be effectively tuned by using the intermediate quantum dot 3. As the energy level of the quantum dot 3 changes, a three-peak structure may evolve into a two-peak structure in the linear conductance spectrum. When the energy levels of quantum dots in arms are not aligned with one another, two Fano dips may appear in the double-quantum-ring device. Two Fano peaks can be effectively modified by tuning the energy level of quantum dot 3. The AB oscillation for magnetic flux is also studied in this work. Our results show that the AB oscillating behavior depends strongly on the difference between the magnetic fluxes threading the left and right rings. In addition to the general AB oscillation with 2π-period, an AB oscillation with π-period can be developed when the difference between the two magnetic fluxes is $(2n + 1)\pi(n = 0, 1, 2,\ldots)$.

Model and Methods

The parallel-coupled quantum-dot structure that we consider is illustrated in Fig. 1. For simplicity, the interdot and intradot coulomb interactions are neglected, and the total Hamiltonian describing the quantum system is written as

$$H = H_{\text{leads}} + H_{\text{DAB}} + H_T, \tag{1}$$

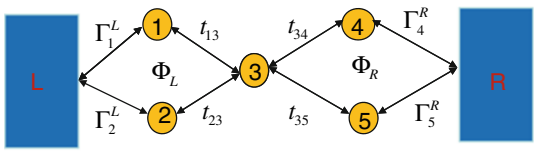

Fig. 1 Schematic plot of a double-Aharonov-Bohm interferometer consisting of five quantum dots sandwiched between two metallic electrodes. The *left ring* encloses a magnetic flux Φ_L, and the *right ring* encloses a magnetic flux Φ_R

where the first term H_{leads} in Eq. (1) describes the left and right electrodes in the noninteracting electron approximation

$$H_{\text{leads}} = \sum_{\alpha=L,R;k} \epsilon_{\alpha k} a_{\alpha k}^{\dagger} a_{\alpha k}, \tag{2}$$

where $a_{\alpha k}^{\dagger}(a_{\alpha k})$ denotes the creation(annihilation) operator for an electron with energy $\varepsilon_{\alpha k}$ and momentum k in electrode α. The second term in Eq. (1) describes the dynamics of the five parallel-coupled quantum dots, which can be modeled by using the following five-site Hamiltonian

$$\begin{aligned} H_{\text{DAB}} = &\sum_{j=1}^{5} \epsilon_j d_j^{\dagger} d_j - (t_{13} e^{-i\phi_L/4} d_1^{\dagger} d_3 + t_{23} e^{i\phi_L/4} d_2^{\dagger} d_3 \\ &+ t_{34} e^{-i\phi_R/4} d_3^{\dagger} d_4 + t_{35} e^{i\phi_R/4} d_3^{\dagger} d_5 + h.c.), \end{aligned} \tag{3}$$

where $d_j^{\dagger}(d_j)$ creates (annihilates) an electron with the energy ε_j in the jth quantum dot, and the AB phase $\phi_\alpha = 2\pi\Phi_\alpha/\Phi_0(\alpha = L, R)$ and the flux quantum $\Phi_0 = h/e$. t_{ij} describes the interdot tunneling coupling between the dot i and dot j, for convenience, which is regarded as a real number. The third term in Eq. (1) describing the tunneling coupling between the quantum dots and the electrodes is divided into two parts

$$H_T = H_T^L + H_T^R. \tag{4}$$

H_T^{α} describes the tunneling coupling between the isolated quantum dots and the electrode α

$$H_T^L = \sum_k [(V_{L1} d_1^{\dagger} + V_{L2} d_2^{\dagger}) a_{Lk} + H.c.], \tag{5}$$

and

$$H_T^R = \sum_k [(V_{R4} d_4^{\dagger} + V_{R5} d_5^{\dagger}) a_{Rk} + H.c.]. \tag{6}$$

A phase factor is attached to $V_{\alpha j}$ in the presence of the magnetic flux, and they can be written as $V_{L1} = |V_{L1}|e^{i\phi_L/4}$, $V_{L2} = |V_{L2}|e^{-i\phi_L/4}$, $V_{R4} = |V_{R4}|e^{-i\phi_R/4}$, $V_{R5} = |V_{R5}|e^{i\phi_R/4}$. In order to study the transport through the double-quantum ring, we need know the retarded (advanced) Green's function $G_{ij}^{r(a)}(\epsilon)$. The retarded Green's function is defined as

$$G_{ij}^{r}(\epsilon) = \ll d_i | d_j^{\dagger} \gg_{\epsilon}^{r} (i, j = 1, 2, 3, 4, 5). \tag{7}$$

Applying the equation of motion method, we obtain a series of equations [32],

$$\begin{aligned} (\epsilon - \epsilon_1) G_{11}^{r}(\epsilon) = &1 - t_{13} e^{-i\phi_L/4} G_{31}^{r}(\epsilon) \\ &+ \sum_k V_{L1} \ll a_{Lk} | d_1^{\dagger} \gg_{\epsilon}^{r}, \end{aligned} \tag{8}$$

$$\begin{aligned} (\epsilon - \epsilon_2) G_{22}^{r}(\epsilon) = &1 - t_{23} e^{i\phi_L/4} G_{32}^{r}(\epsilon) \\ &+ \sum_k V_{L2} \ll a_{Lk} | d_2^{\dagger} \gg_{\epsilon}^{r}, \end{aligned} \tag{9}$$

$$(\epsilon-\epsilon_3)G^r_{33}(\epsilon)=1-t_{13}e^{i\phi_L/4}G^r_{13}(\epsilon)-t_{23}e^{-i\phi_L/4}G^r_{32}(\epsilon)-t_{34}e^{-i\phi_R/4}G^r_{43}(\epsilon)-t_{35}e^{i\phi_R/4}G^r_{53}(\epsilon), \quad (10)$$

$$(\epsilon-\epsilon_4)G^r_{44}(\epsilon)=1-t_{34}e^{i\phi_R/4}G^r_{34}(\epsilon)+\sum_k V_{R4}\ll a_{Rk}|d_4^\dagger\gg^r_\epsilon, \quad (11)$$

$$(\epsilon-\epsilon_5)G^r_{55}(\epsilon)=1-t_{35}e^{-i\phi_R/4}G^r_{35}(\epsilon)+\sum_k V_{R5}\ll a_{Rk}|d_5^\dagger\gg^r_\epsilon . \quad (12)$$

Four new Green's functions arising from the tunneling couplings between the quantum dots and metallic electrodes appear in the above Eqs. (8–9) and Eqs. (11–12), and they are

$$(\epsilon-\epsilon_{Lk})\ll a_{Lk}|d_1^\dagger\gg^r_\epsilon=V^*_{L1}G^r_{11}(\epsilon)+V^*_{L2}G^r_{21}(\epsilon), \quad (13)$$

$$(\epsilon-\epsilon_{Lk})\ll a_{Lk}|d_2^\dagger\gg^r_\epsilon=V^*_{L1}G^r_{12}(\epsilon)+V^*_{L2}G^r_{22}(\epsilon), \quad (14)$$

$$(\epsilon-\epsilon_{Rk})\ll a_{Rk}|d_4^\dagger\gg^r_\epsilon=V^*_{R4}G^r_{44}(\epsilon)+V^*_{R5}G^r_{54}(\epsilon), \quad (15)$$

$$(\epsilon-\epsilon_{Rk})\ll a_{Rk}|d_5^\dagger\gg^r_\epsilon=V^*_{R4}G^r_{45}(\epsilon)+V^*_{R5}G^r_{55}(\epsilon). \quad (16)$$

Using the above Eqs. (8–16), the retarded Green's function $\boldsymbol{G}^r$ can be calculated by the following 5×5 matrix

$$\mathbf{G}^r=\begin{pmatrix} g_1 & \frac{i}{2}\sqrt{\Gamma^L_1\Gamma^L_2}e^{i\phi_L/2} & t_{13}e^{-i\phi_L/4} & 0 & 0\\ \frac{i}{2}\sqrt{\Gamma^L_1\Gamma^L_2}e^{i\phi_L/2} & g_2 & t_{23}e^{i\phi_L/4} & 0 & 0\\ t_{13}e^{i\phi_L/4} & t_{23}e^{-i\phi_L/4} & \epsilon-\epsilon_3 & t_{34}e^{-i\phi_R/4} & t_{35}e^{i\phi_R/4}\\ 0 & 0 & t_{34}e^{i\phi_R/4} & g_4 & \frac{i}{2}\sqrt{\Gamma^R_4\Gamma^R_5}e^{-i\phi_R/2}\\ 0 & 0 & t_{35}e^{-i\phi_R/4} & \frac{i}{2}\sqrt{\Gamma^R_4\Gamma^R_5}e^{i\phi_R/2} & g_5 \end{pmatrix}^{-1}, \quad (17)$$

where $g_j=\epsilon-\epsilon_j+\frac{i}{2}\Gamma^\alpha_j$ and $\Gamma^\alpha_j=\sum_k|V_{\alpha j}|^2 2\pi\delta(\epsilon-\epsilon_{\alpha k})$ ($j=1,2$ for $\alpha=L$; $j=4,5$ for $\alpha=R$). The advanced Green's function $\mathbf{G}^a$ is obtained by the relation $G^a_{ij}=G^{r*}_{ji}$. The linear conductance of the double quantum ring at zero temperature can be calculated by the Landauer Formula [32],

$$\sigma=\frac{2e^2}{h}Tr[\Gamma^L\mathbf{G}^r\Gamma^R\mathbf{G}^a]. \quad (18)$$

The linewidth matrices Γ^L and Γ^R are given

$$\Gamma^L=\begin{pmatrix} \Gamma^L_1 & \sqrt{\Gamma^L_1\Gamma^L_2}e^{i\phi_L/2} & 0 & 0 & 0\\ \sqrt{\Gamma^L_1\Gamma^L_2}e^{-i\phi_L/2} & \Gamma^L_2 & 0 & 0 & 0\\ 0 & 0 & 0 & 0 & 0\\ 0 & 0 & 0 & 0 & 0\\ 0 & 0 & 0 & 0 & 0 \end{pmatrix} \quad (19)$$

and

$$\Gamma^R=\begin{pmatrix} 0 & 0 & 0 & 0 & 0\\ 0 & 0 & 0 & 0 & 0\\ 0 & 0 & 0 & 0 & 0\\ 0 & 0 & 0 & \Gamma^R_4 & \sqrt{\Gamma^R_4\Gamma^R_5}e^{-i\phi_R/2}\\ 0 & 0 & 0 & \sqrt{\Gamma^R_4\Gamma^R_5}e^{i\phi_R/2} & \Gamma^R_5 \end{pmatrix}. \quad (20)$$

In the case of the symmetrical dot-electrode tunneling couplings ($\Gamma^L_1=\Gamma^L_2=\Gamma^R_4=\Gamma^R_5=\Gamma$), the linear conductance has the following form,

$$\sigma=\frac{2e^2\Gamma^2}{h}\Big\{\sum_{m=1,2;n=4,5}|G^r_{mn}|^2+2Re\Big[G^r_{14}\Big(G^a_{51}e^{-i\frac{\phi_R}{2}}+G^a_{42}e^{-i\frac{\phi_L}{2}}\Big)+G^r_{25}\Big(G^a_{42}e^{i\frac{\phi_R}{2}}+G^a_{51}e^{i\frac{\phi_L}{2}}\Big)+G^r_{25}G^a_{41}e^{i\bar{\phi}}+G^r_{24}G^a_{51}e^{i\frac{\Delta\phi}{2}}\Big]\Big\}, \quad (21)$$

where $\bar{\phi}=(\phi_L+\phi_R)/2$ and $\Delta\phi=(\phi_L-\phi_R)$. From the above equation, we note that the linear conductance includes the contributions from four different electron tunneling paths ($1\to3\to4$, $1\to3\to5$, $2\to3\to4$;$2\to3\to5$) and interference terms among them. Equation (21) is also written as:

$$\sigma=\frac{2e^2\Gamma^2}{h}|G^r_{14}e^{-\frac{i}{4}(\phi_L+\phi_R)}+G^r_{15}e^{\frac{i}{4}(\phi_R-\phi_L)}+G^r_{24}e^{\frac{i}{4}(\phi_L-\phi_R)}+G^r_{25}e^{\frac{i}{4}(\phi_L+\phi_R)}|^2. \quad (22)$$

Results and Discussion

In this section, the dependence of the linear conductance σ on system parameters is discussed numerically and analytically. The coupling strength between the quantum dots and the metallic electrodes Γ is taken as the energy unit. Through this paper, all energy levels in quantum dots, tunneling couplings and Fermi energy are measured by Γ.

Without Magnetic Flux

We first study the linear transport properties of the double-AB interferometer consisting of five parallel-coupled

quantum dots with the same energy levels ($\varepsilon_j = 0$, $j = 1, 2, 3, 4, 5$) in the absence of the magnetic fluxes ($\phi_L = \phi_R = 0$). Figure 2a shows the linear conductance σ of the double-quantum-ring structure as a function of the Fermi level E_F in the case of symmetrical interdot tunneling couplings. The same interdot tunneling coupling strengths are chosen as $t_{13} = t_{23} = t_{34} = t_{35} = t$. There are total five molecular states in center five-dot quantum system, but three molecular states of which with zero energy are degenerate. Other two molecular states are located at $-2t$ and $2t$, respectively. So we find that there are three resonance peaks with $\sigma = 2e^2/h$ appearing at 0, $2t$ and $-2t$, respectively. With t increasing, the position of the center conductance peak has no changing, while the other two conductance peaks move in the opposite direction as shown in Fig. 2a. In Fig. 2b and c, we display the linear conductance σ as a function of the Fermi energy E_F in the case of asymmetrical interdot tunneling couplings. In Fig. 2b, we assume the interdot tunneling coupling strengths as $t_{13} = t_{23} = 2\Gamma$ and $t_{34} = t_{35}$. In this case, three conductance peaks are located at 0, $\sqrt{2(t_{13}^2 + t_{34}^2)}$, and $-\sqrt{2(t_{13}^2 + t_{34}^2)}$, respectively. As t_{34} decreases, the conductance peaks are suppressed and become narrower as shown in Fig. 2b. In Fig. 2c, we examine the transport properties of the double-quantum-ring structure by tuning t_{23} and t_{34}. Here we fix the interdot tunneling couplings t_{13} and t_{35} at 2Γ. A Fano dip (zero conductance point) appears at $E_F = 0$ when t_{23} (t_{34}) is different from $t_{13}(t_{35})$. The behind reason is the destructive interference effects between the electron waves directly transmitting through the three coupled quantum dots in series and side-coupled quantum dots (see the inset in Fig. 2c). As t_{23} and t_{34} decrease, a three-peak structure in the linear conductance spectrum evolves into the four-peak structure. When $t_{23} = t_{34} = 0$, the quantum device becomes a three quantum-dot array sandwiched between two metallic electrodes with side-coupled quantum dots as shown in the inset of Fig. 2c. The Fano dip is located at the energy levels of the side-coupled quantum dots ($\varepsilon_2 = \varepsilon_4 = 0$). It is noted that two peaks become closer and narrower as t_{23} and t_{34} decrease. When $t_{23} = t_{34} = 0$, the two conductance peaks are located at $\pm\sqrt{2}t_{13}(t_{35})$.

Figure 3 displays the linear conductance σ as a function of E_F when the energy level of the third quantum dot ε_3 is not aligned with those of the other four quantum dots. Five molecular states appear at $0, 0, 0, \frac{1}{2}\left(\epsilon_3 - \sqrt{\epsilon_3^2 + 16\Gamma^2}\right), \frac{1}{2}\left(\epsilon_3 + \sqrt{\epsilon_3^2 + 16\Gamma^2}\right)$, respectively. When $\varepsilon_3 = 0$, three conductance peaks with $\sigma = 2e^2/h$ are centered at 0, 2Γ and -2Γ, respectively. The linear conductance σ as a function of E_F under the different values of ε_3 is plotted in Fig. 3a and b. The left two conductance peaks evolve into a single conductance peak, and the right conductance peak moves in the right direction in the case of $\varepsilon_3 > 0$. We also find the height of the left conductance peak is suppressed. In the case of $\varepsilon_3 < 0$, the situation is in inverse. The right two conductance peaks evolve into a single conductance peak, and the height of the conductance peak is suppressed. The left conductance peak moves in the left direction, and the height of the conductance peak has no changing. In order to explore the dependence of the linear conductance on the energy level of the intermediate

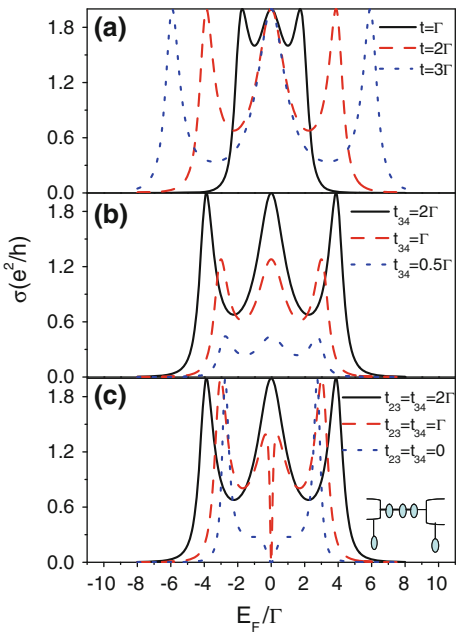

Fig. 2 Linear conductance σ as a function of E_F under different interdot tunneling couplings. The energy levels of the quantum dots are chosen as $\varepsilon_1 = \varepsilon_2 = \varepsilon_3 = \varepsilon_4 = \varepsilon_5 = 0$

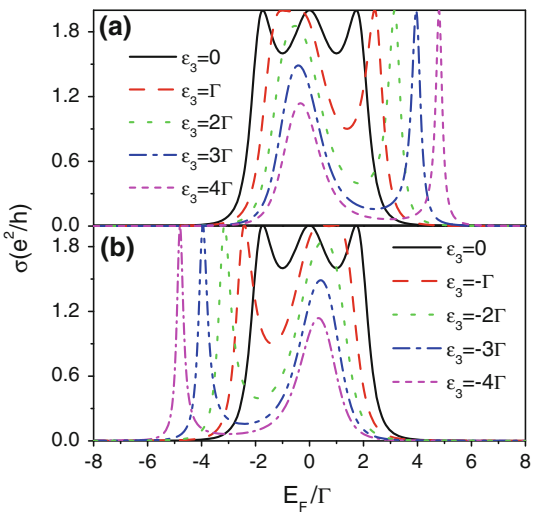

Fig. 3 Linear conductance σ as a function of the Fermi energy level E_F in **a** the case of $\varepsilon_3 > 0$; **b** the case of $\varepsilon_3 < 0$. Other system parameters are chosen as in Fig. 2

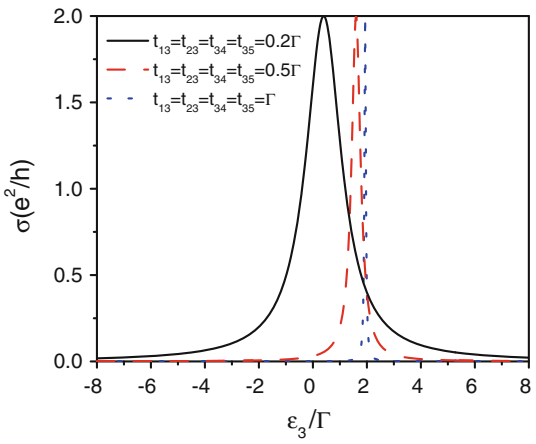

Fig. 4 Linear conductance σ as a function of the energy level of the quantum dot 3 in the presence of different interdot tunneling coupling strengths. Other system parameters are chosen as in Fig. 2

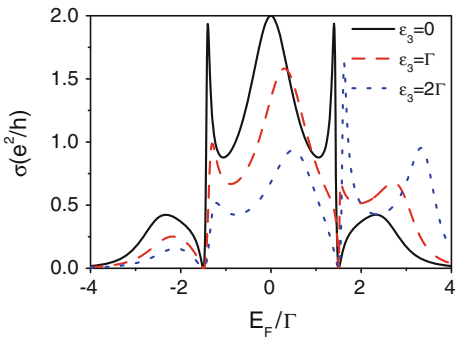

Fig. 5 Linear conductance σ as a function of the Fermi energy E_F under several different values of the quantum dot 3. Other quantum-dot energy levels are chosen as $\epsilon_1 = -2\Gamma$, $\epsilon_2 = -\Gamma$, $\epsilon_4 = \Gamma$ and $\epsilon_5 = 2\Gamma$, respectively

quantum dot 3, we plot the linear conductance as a function of ε_3 under several different interdot couplings in Fig. 4. With ε_3 increasing, the linear conductance first increases and reaches the maximum value at the certain value ε_{3m}. When the interdot couplings become small, ε_{3m} moves toward the Fermi energy. Once the interdot couplings are enough small, the resonant conductance peak is almost pined at E_F. The transport properties of the double-quantum ring are similar with these of a single quantum dot coupled straightly to metallic electrodes.

In Fig. 5, we study the transport properties of the double-quantum ring when the quantum-dot levels are not aligned with one another. The same interdot coupling strengths ($t_{13} = t_{23} = t_{34} = t_{35} = t = \Gamma$) are considered, and the energy levels of quantum dots parameters are chosen as $\epsilon_1 = -2\Gamma, \epsilon_2 = -\Gamma$, $\epsilon_4 = \Gamma$ and $\epsilon_5 = 2\Gamma$, respectively. Since the degenerate states are opened in this case, five conductance peaks appear in the linear conductance spectrum. The linear conductance σ consists of three Breit-Wigner peaks and two sharp asymmetric Fano peaks. A Fano dip happens at $\frac{\epsilon_1+\epsilon_2}{2}$, while the other Fano dip appears at $\frac{\epsilon_4+\epsilon_5}{2}$. The numerical results may be explained by using Eq. (21). The linear conductance in the absence of magnetic flux can be written as

$$\sigma = \frac{2e^2\Gamma^2}{h}|G^r_{14} + G^r_{24} + G^r_{25} + G^r_{15}|^2. \tag{23}$$

Using Eq. (17), we arrive at

$$\sigma = \frac{2e^2\Gamma^2}{h}\frac{t^4(2E_F - \epsilon_1 - \epsilon_2)^2(2E_F - \epsilon_4 - \epsilon_5)^2}{|det[G^r]^{-1}|^2}. \tag{24}$$

From the above equation, we see clearly $\sigma = 0$ for $E_F = \frac{\epsilon_1+\epsilon_2}{2}$ or $E_F = \frac{\epsilon_4+\epsilon_5}{2}$. The linear conductance spectrum has mirror symmetry around ε_3 in the case of $\varepsilon_3 = 0$. With increasing ε_3, the mirror symmetry is broken. The left Fano peak is suppressed, while the right Fano peak is firstly suppressed, then it is enhanced.

With Magnetic Flux

The periodic oscillation in the linear conductance for the magnetic flux is key features when the phase coherence of the electrons is preserved. In this section, we start with the study of dependence of the linear conductance on the magnetic fluxes through the double-quantum ring. The dependence of the linear conductance on the Fermi energy in the presence of the same magnetic flux through the left and right rings ($\phi_L = \phi_R = \phi$) is shown in Fig. 6. The same interdot tunneling couplings ($t_{13} = t_{23} = t_{34} = t_{35} = \Gamma$) and the same quantum-dot energy levels $\varepsilon_1 = \varepsilon_2 = \varepsilon_3 = \varepsilon_4 = \varepsilon_5 = \varepsilon_0 = 0$ are considered. When the magnetic flux ϕ is presented, a Fano dip is developed when the Fermi energy is aligned with ε_0. With ϕ increasing, the three-peak structure disappears, while a four-peak structure in the linear conductance spectrum appears. When the magnetic fluxes are further increased, the four-peak structure evolves into a double-peak structure. The results may be explained by the following expressions. After some algebra, we derive the linear conductance σ in the presence of the magnetic flux as the following analytical form

$$\sigma(E_F, \phi) = \frac{2e^2\Gamma^2}{h}\frac{4E_F^2\Gamma^4[1 + \cos(\phi)]^2}{(E_F^2 + \Gamma^2)\{E_F^2(E_F^2 - 4\Gamma^2)^2 + \Gamma^2[E_F^2 - 2\Gamma^2 + 2cos(\phi)\Gamma^2]^2\}}, \tag{25}$$

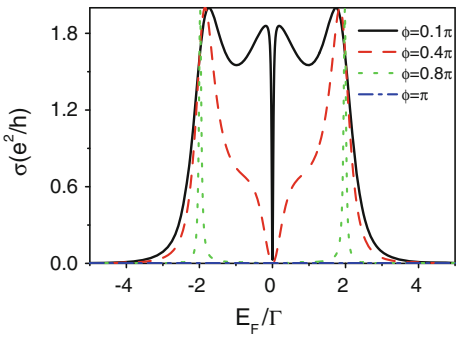

Fig. 6 Linear conductance σ as a function of the Fermi energy E_F under several different magnetic fluxes threading the *left* and *right rings* $\phi_L = \phi_R = \phi$

From the above equation, we see clearly that the linear conductance disappears when $E_F = 0$, and four molecular states are located around $\pm 2\Gamma$ and $\pm\sqrt{2 - 2cos(\phi)}\Gamma$, respectively. With ϕ increasing, the two middle conductance peaks are suppressed obviously, while the outside conductance peaks become shaper as shown in Fig. 6. When ϕ approaches π, we can obtain an approximate formula for the linear conductance

$$\sigma \simeq \frac{2e^2\Gamma^2}{h} \frac{4E_F^2\Gamma^4\delta_1}{(E_F^2+\Gamma^2)[2E_F^2(E_F^2-4\Gamma^2)^2+\delta_2]}, \tag{26}$$

where δ_1 and δ_2 represent two small quantities. Equation (26) shows two narrower conductance peaks are centered at $\pm 2\Gamma$ as shown in Fig. 6. When $\phi = n\pi$(n is odd number), the linear conductance disappears everywhere for any value of E_F.

Figure 7 shows the images of the linear conductance σ as functions of ϕ_L and the Fermi energy E_F. The same interdot couplings and same quantum-dot levels are considered. $\Delta\phi = \phi_L - \phi_R$ denotes the difference between magnetic fluxes through the left quantum ring and right quantum ring. When $\Delta\phi \neq (2n+1)\pi$, a general 2π-periodic AB oscillation for ϕ_L is obtained as shown in Fig. 7a and b. When $\Delta\phi = (2n+1)\pi$, a π-periodic AB oscillation appears in the quantum system as shown in Fig. 7c. The above results can be explained as following expressions. When the magnetic fluxes through the double-quantum ring are considered, using Eq. (24), we arrive at

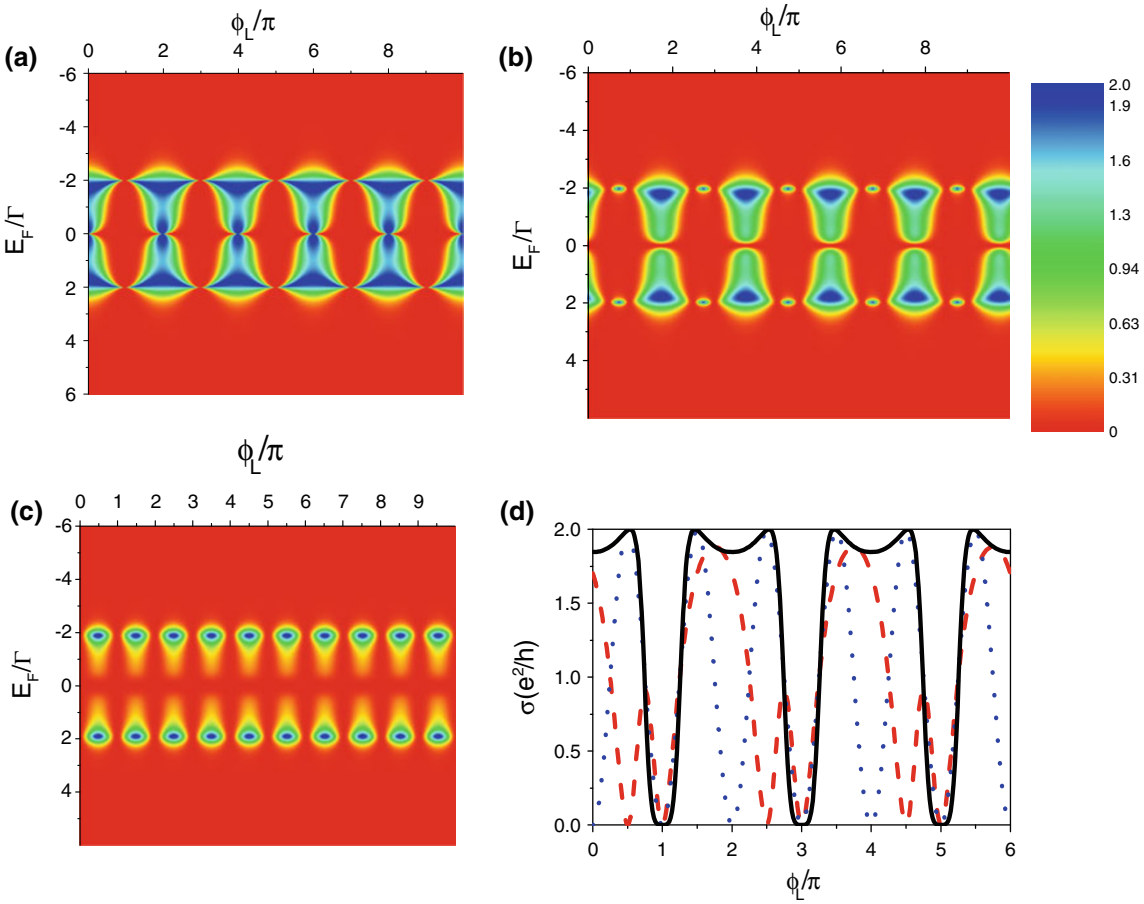

Fig. 7 Images of the linear conductance σ as functions of the fermi energy E_F and ϕ_L for **a** $\Delta\phi = 0$, **b** $\Delta\phi = 0.5\pi$, and **c** $\Delta\phi = \pi$, respectively. **d** Linear conductance σ as a function of magnetic flux ϕ_L for $\Delta\phi = 0$ [*solid (black) line*], $\Delta\phi = 0.5\pi$ [*dashed (red) line*], and $\Delta\phi = \pi$ [*dotted (blue) line*], respectively. Other system parameters are chosen as in Fig. 6

When $\phi_R - \phi_L = \Delta\phi = \pi$, the above equation can be simplified as

$$\sigma = \frac{2e^2\Gamma^2}{h}\frac{16E_F^2\Gamma^4 cos^2(\frac{\phi_L}{2})\cos^2(\frac{\phi_R}{2})}{(E_F^2+\Gamma^2)\{E_F^2(E_F^2-4\Gamma^2)^2+\Gamma^2[E_F^2-2\Gamma^2+\cos(\phi_L)\Gamma^2+\cos(\phi_R)\Gamma^2]^2\}}. \quad (27)$$

$$\sigma = \frac{2e^2\Gamma^2}{h}\frac{2E_F^2\Gamma^4[1-\cos(2\phi_L)]}{(E_F^2+\Gamma^2)[E_F^2(E_F^2-4\Gamma^2)^2+\Gamma^2(E_F^2-2\Gamma^2)^2]}. \quad (28)$$

So an AB oscillation with π-period is developed as shown in Fig. 7c and d.

It is well known that an oscillating current in the AB interferometer has been detected experimentally [8, 9]. For a single quantum ring consisting of two parallel-coupled quantum dots sandwiched between two metallic electrodes, 2π-periodic oscillation of the linear conductance σ is reported in the pervious works [13]. The linear conductance σ as a function of ϕ_L under the different energy levels in the quantum dot 3 or several different values of ϕ_R is shown in Fig. 8. The Fermi energy E_F is fixed at 0.2Γ, and other system parameters are chosen as in Fig. 6. The AB oscillation for ϕ_L in the presence of different energy levels of the quantum dot 3 is potted in Fig. 8a. For $\varepsilon_3 = 0$, a series of shaper resonant peaks appear at $2n\pi(n = 0, 1, 2\ldots)$, and the linear conductance reaches a minimum ($\sigma = 0$) when ϕ_L approaches $(2n + 1)\pi(n = 0, 1, 2\ldots)$. When the energy level in quantum dot 3 is not aligned with other quantum-dot levels, the single conductance peak around $2n\pi$ splits into the two conductance peaks. With ε_3 moving away from zero energy point, two conductance peaks move in the opposite direction. It is noted that the double-peak structure around $2n\pi$ disappears slowly as the magnetic flux threading the right quantum ring increases.

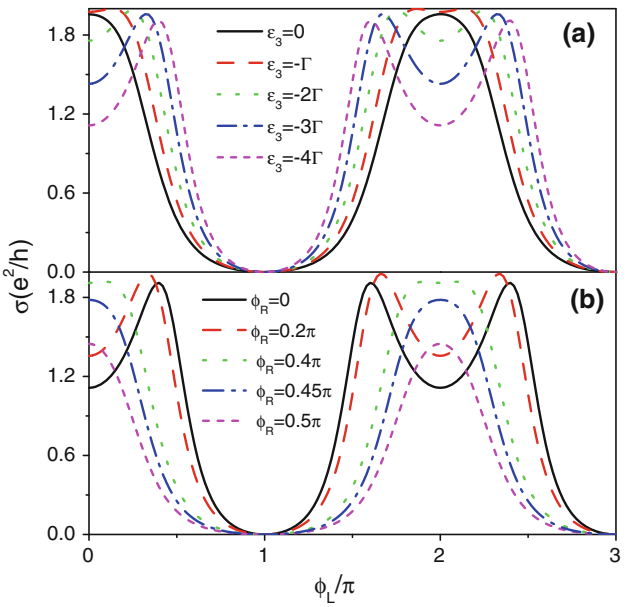

Fig. 8 **a** AB oscillations for ϕ_L in the presence of several different energy levels of the quantum dot 3 with $\phi_R = 0$; **b** AB oscillations for ϕ_L in the presence of several different magnetic fluxes ϕ_R with the fixed $\epsilon_3 = -4\Gamma$. Other system parameters are chosen as $\varepsilon_1 = \varepsilon_2 = \varepsilon_4 = \varepsilon_5 = 0$, $t_{13} = t_{23} = t_{34} = t_{35} = \Gamma$, and $E_F = 0.2\Gamma$

Summary

In summary, the transport properties and quantum interference effects in a double-AB interferometer in series consisting of five quantum dots in the case of symmetric dot-electrode tunneling couplings are studied by using Green's function equation of motion method. The energy levels of all quantum dots can be tuned by the voltages applied on the quantum dots in experiments. The linear conductance can be effectively modified by the intermediate quantum dot 3. As the energy level in the quantum dot 3 changes, a three-peak structure in the linear conductance spectrum evolves into a two-peak structure. When the quantum-dot levels in arms are not aligned with one another, two Fano resonances with different Fano factors may appear in the quantum device. The AB oscillation for the magnetic flux in the double-AB interferometer is also studied in this work. The results show that the AB oscillating behavior depends strongly on the difference between the magnetic fluxes threading the left and right quantum rings. An AB oscillation with π-period for the magnetic flux threading the left quantum ring is developed when the difference between the two magnetic fluxes is $(2n + 1)\pi(n = 0, 1, 2,\ldots)$.

Acknowledgments The authors thank the supports of the National Natural Science Foundation of China (NSFC) under Grant No. 10947130 and the Science Foundation of the Education Committee of Jiangsu Province under Grant No. 09KJB140001. The authors also thank the supports of the Foundations of Changshu Institute of Technology.

References

1. D. Goldhaber-Gordon, H. Shtrikman, D. Mahalu, D. Abusch-Magder, U. Meirav, M.A. Kastner, Nature (London) **391**, 156 (1998)
2. W.G. Vanderwiel, S.D. Franceschi, J.M. Elgerman, S.Tarucha, L.P. Kouwenhoven, Rev. Mod. Phys. **75**, 1 (2003)
3. N.D. Lang, Phys. Rev. B **52**, 5335 (1995).
4. M. Di Ventra, N.D. Lang, Phys. Rev. B **65**, 045402 (2001)
5. Y.S. Liu, H. Chen, X.H. Fan, X.F. Yang, Phys. Rev. B **73**, 115310 (2006)
6. Y.S. Liu, X.F. Yang, X.J. Xia, Solid State Commun. **146**, 502 (2008)
7. K. Kobayashi, H. Aikawa, S. Katsumoto, Y. Iye, Phys. Rev. Lett. **88**, 256806 (2002)
8. A.W. Holleitner, R.H. Blick, A.K. Huttel, K. Eberl, J.P. Kotthaus, Science **297**, 70 (2002)
9. A.W. Holleitner, C.R. Decker, H. Qin, K. Eberl, R.H. Blick, Phys. Rev. Lett. **87**, 256802 (2001)
10. A.A. Clerk, X. Waintal, P.W. Brouwer, Phys. Rev. Lett. **86**, 4636 (2001)
11. M.L. Ladrón de Guevara, F. Claro, P.A. Orellana, Phys. Rev. B **67**, 195335 (2003)
12. Z.Y. Zeng, F. Claro, Phys. Rev. B **65**, 193405 (2002)
13. B. Kubala, J. König, Phys. Rev. B **65** 245301 (2002)
14. Z.M. Bai, M.F. Yang, Y.C. Chen, J. Phys. Condens. Matter. **16**, 2053 (2004)
15. H.Z. Lu, R. Lü, B.F. Zhu, Phys. Rev. B **71**, 235320 (2005)
16. Y.S. Liu, H. Chen, X.F. Yang, J. Phys. Condens. Matter. **19**, 246201 (2007)
17. F. Chi, S.S. Li, J. Appl. Phys. **97**, 123704 (2005)
18. F. Chi, S.S. Li, J. Appl. Phys. **99**, 043705 (2006)
19. K.W. Chen, C.R. Chang, J. Appl. Phys. **103**, 07B705 (2008)
20. K.W. Chen, C.R. Chang, Phys. Rev. B **78**, 235319 (2008)
21. B.H. Wu, J.C. Cao, J. Phys. Condens. Matter. **16**, 8285 (2004)
22. S. Tanaka, S. Garmon, G. Ordonez, T. Petrosky, Phys. Rev. B **76**, 153308 (2007)
23. Z.Y. Zeng, F. Claro, A. Pérez, Phys. Rev. B **65**, 085308 (2002)
24. M.L. Ladron de Guevara, P. Orellana, Phys. Rev. B **73**, 205303 (2006)
25. Y.X. Li, J. Phys. Condens. Matter. **19**, 496219 (2007)
26. Y.S. Liu, X.F. Yang, X. Zhang, Y.J. Xia, Phys. Lett. A **372**, 3318 (2008)
27. R. Wang, J.Q. Liang, Phys. Rev. B **74**, 144302 (2006)
28. W.J. Gong, Y.S. Zheng, Y. Liu, T.Q. Lü, Phys. Rev. B **73**, 245329 (2006)
29. W.J. Gong, C. Jiang, J. Appl. Phys. **103**, 07B705 (2008)
30. F. Zhai, H.Q. Xu, Phys. Rev. B **72**, 195346 (2005)
31. S. Jana, A. Chakrabarti, Phys. Rev. B **77**, 155310 (2008)
32. H. Haug, A.-P. Jauho, Quantum Kinetics in Transport and Optics of Semiconductors, 2nd edn. (Springer, Berlin, 2007)